SCIENTIFIC REPORTS

OPEN

SUBJECT AREAS:
MATERIALS SCIENCE
CATALYSIS
CHEMICAL PHYSICS
PLASMA PHYSICS

Received
9 September 2011

Accepted
24 October 2011

Published
14 November 2011

Correspondence and requests for materials should be addressed to Z.H.Z. (z.zhu@uq.edu.au)

* These authors contributed equally to this work.

Heterostructured electrode with concentration gradient shell for highly efficient oxygen reduction at low temperature

Wei Zhou[1]*, Fengli Liang[1]*, Zongping Shao[2], Jiuling Chen[1] & Zhonghua Zhu[1]

[1]Division of Chemical Engineering, The University of Queensland, Brisbane, Queensland 4072, Australia, [2]State Key Laboratory of Materials-Oriented Chemical Engineering, College of Chemistry & Chemical Engineering, Nanjing University of Technology, No.5 Xin Mofan Road, Nanjing 210009, PR China.

Heterostructures of oxides have been widely investigated in optical, catalytic and electrochemical applications, because the heterostructured interfaces exhibit pronouncedly different transport, charge, and reactivity characteristics compared to the bulk of the oxides. Here we fabricated a three-dimensional (3D) heterostructured electrode with a concentration gradient shell. The concentration gradient shell with the composition of $Ba_{0.5-x}Sr_{0.5-y}Co_{0.8}Fe_{0.2}O_{3-\delta}$ (BSCF-D) was prepared by simply treating porous $Ba_{0.5}Sr_{0.5}Co_{0.8}Fe_{0.2}O_{3-\delta}$ (BSCF) backbone with microwave-plasma. Electrochemical impedance spectroscopy reveals that the oxygen surface exchange rate of the BSCF-D is enhanced by ~250% that of the pristine BSCF due to the appearance of the shell. The heterostructured electrode shows an interfacial resistance as low as 0.148 Ω cm² at 550°C and an unchanged electrochemical performance after heating treatment for 200 h. This method offers potential to prepare heterostructured oxides not only for electrochemical devices but also for many other applications that use ceramic materials.

Solid oxide fuel cells (SOFCs) is a promising technology in power generation because of their high energy efficiency and negligible impact on environment[1–3]. Conventional SOFC systems operating in the temperature region of 800–1000°C are restricted to large-scale stationary applications. In the last decades, reducing the operation temperature of SOFCs is a hot topic on their commercialization[4–6]. At low operating temperature (500–700°C) small-scale applications and even portable devices can be achieved, which opens more opportunities for SOFCs[7].

However, low electrocatalytic activity of cathode is still a major challenge facing low-temperature SOFCs. Composite metal oxides, possessing ABO_3 perovskite structure, is attracting considerable attentions, because the physical and chemical properties of the oxides are tuneable by partial substitution of cations in positions A and/or B[8]. Moreover, the capability of tolerating large oxygen or cation nonstoichiometry in their lattice accounts for tailoring the perovskite structured oxides into high performance cathodes[9]. Some perovskite cathodes readily show high electrocatalytic activity (i.e. low interfacial resistance, <0.15 Ω cm²) on oxygen reduction reaction (ORR) at 700~800°C[10–12], but the cathodes that work at low temperatures (<600°C) are rarely reported.

The cathode of SOFCs is used to catalytically reduce oxygen to oxygen anions. Some experiments and numerical studies have shown that oxygen surface process plays an important role in the ORR[13,14]. For example, in 2000, Shao and Haile reported a high performance perovskite cathode with a composition of $Ba_{0.5}Sr_{0.5}Co_{0.8}Fe_{0.2}O_{3-\delta}$ (BSCF), which allows SOFCs to work with high power density at 600°C[15]. The high activity of BSCF can be ascribed to the highly improved oxygen surface exchange rate, as a fact that the electrochemical surface exchange resistance of BSCF is more than a factor of 50 lower than the value for $La_{0.6}Sr_{0.4}Co_{0.8}Fe_{0.2}O_{3-\delta}$ (LSCF) reported by Baumann et al. (refs. 16). A large number of methods have been tried to optimize the BSCF cathode by modifying its surface[17–21]. Among those methods, introduction of A-site cations deficiency into BSCF has shown improved properties in oxygen surface exchange[17,18]. However, the phase reaction between A-site deficient BSCF cathode and electrolyte becomes more serious at a higher level of cation deficiency[18]. The new phases, which are readily formed in the cathode fabrication process (at 1000°C), may block

the ionic transport at the cathode|electrolyte interface, thus increase the interfacial resistance of the cathode[18]. Even though the phase reaction can be alleviated by reducing sintering temperature of cathode fabrication, the poor connection between cathode and electrolyte due to undersintering may also increase the interfacial resistance of cathode. This conflict makes A-site deficient BSCF difficult to be used based on a conventional cathode fabrication process. The lowered electrical conductivity of A-site deficient BSCF also restricts its practical application.

We have been working on coating the BSCF cathode with a thin A-site deficient BSCF $Ba_{0.5-x}Sr_{0.5-y}Co_{0.8}Fe_{0.2}O_{3-\delta}$ (BSCF-D) film to form core-shell heterostructured cathode. The oxygen surface exchange would be improved by this shell, while the electrical conductivity of the "core" (BSCF) and the BSCF|SDC interface would not be affected.

The core-shell particles can be synthesized by a number of synthetic methods, such as co-precipitation method, assembly process, and template method[22]. However, if we use the core-shell particles to fabricate the cathode, the reaction between BSCF-D and electrolyte still can not be avoided during the cathode fabrication. Therefore, to achieve the desired core-shell structured cathode, the BSCF backbone (core) has to be sintered to electrolyte before the formation of BSCF-D shell. Heterostructured thin films can be prepared on the flat substrate by physical vapor deposition, such as molecular beam epitaxy (MBE), and pulsed laser deposition (PLD)[23]. However, only 2D structures can be obtained from these techniques; and the processes are complicated and costly.

Here, we report a novel 3D heterostructured cathode, consisting of stoichiometric BSCF as the core and concentration gradient BSCF-D as the shell, prepared by simply treating pre-sintered porous BSCF backbone under microwave plasma (**Figure 1**). To the best of our knowledge, it is the first time to use microwave plasma to prepare such a structured electrode. The treatment is performed on BSCF|SDC|BSCF symmetric cells. The BSCF cathode has been pre-sintered to the SDC electrolyte, so no undesired phase forms at the cathode|electrolyte interface at this stage. The heterostructured cathode shows significantly enhanced electrocatalytic activity due to the high oxygen surface exchange rate of BSCF-D.

Results

Structure and morphology of the heterostructured electrode. The temperature of BSCF surface reaches as high as ~1800°C under microwave plasma in a few seconds. Ba and Sr at the vicinity of the BSCF surface evaporate from lattice at high temperature to form a BSCF-D shell. The phase structure of the BSCF treated for various time was characterized by x-ray diffraction (XRD) (**Figure S1, supporting information**). The crystallite structure of the samples is obtained by Retvield refinement. All the samples show a cubic structure with Pm–3m (211) space group. The lattice parameter decreases with increasing heating time, indicating the formation of A-site deficient BSCF. It was reported that the lattice shrank after introducing A-site deficiency into BSCF[17]. The lattice parameter of the sample treated for 40 min is 0.3985(6) nm close to the value of $(Ba_{0.5}Sr_{0.5})_{0.91}Co_{0.8}Fe_{0.2}O_{3-\delta}$[18], indicating the A-site deficient concentration is around 0.09 after the treatment. Overheating of BSCF results in deep decomposition of BSCF, additional phase (Co_3O_4) is thus observed after the treatment for 80 min.

The possible phase reaction between BSCF and SDC under microwave plasma treatment was studied by XRD. The samples for XRD characterization were prepared by pressing and sintering BSCF-SDC mixture, and treating the sintered pellets under microwave plasma for up to 80 min. Besides the diffraction peaks indexing to BSCF and SDC, no other peaks can be observed by XRD patterns, indicating negligible phase reaction (**Figure S2, supporting information**).

The surface morphologies of the BSCF cathodes before and after the treatment were observed by field emission scanning electron microscopy (FESEM) and atomic force microscope (AFM). Although very high temperature was used in the microwave plasma treatment, the process does not lead to the sintering of the BSCF grains due to relatively short time, reflected by the unchanged grain size as observed by FESEM (**Figures 2a and 2b**). However, uniformly distributed nano-sized particles (50–70 nm) are formed after treatment (**Figure 3d**). The particles are Ba and Sr enriched phase based on energy dispersive X-ray (EDX) analysis (**Figure S3, supporting information**), verifying the evaporation of Ba and Sr from the BSCF lattice. AFM images of the fresh and treated BSCF

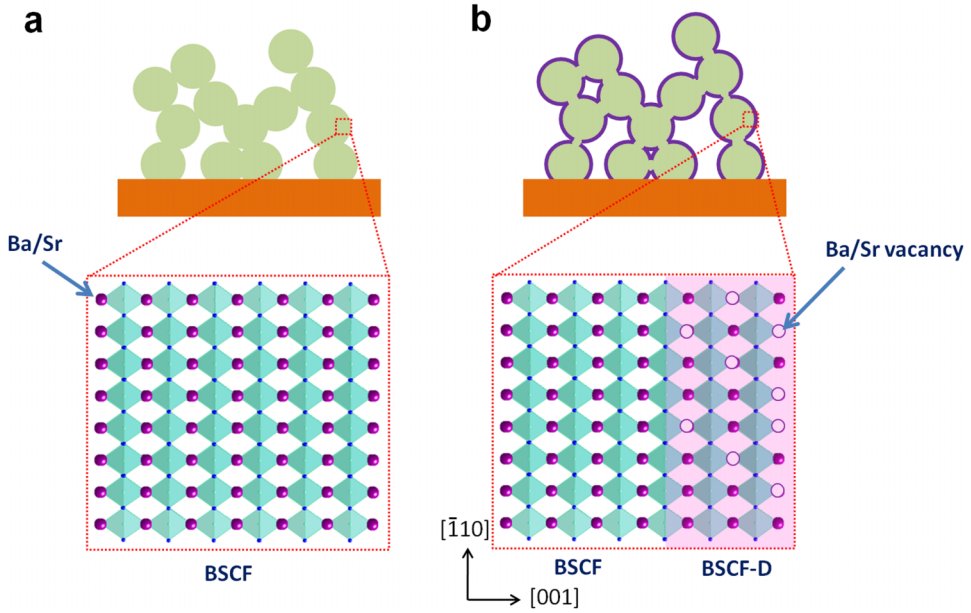

Figure 1 | Schematic of microwave plasma treatment on a BSCF cathode. (a) The porous BSCF backbone can be sintered onto SDC electrolyte by a conventional process without any impurities formed at BSCF|SDC inferface. (b) After the treatment Ba and Sr elements partially evaporate from A-site of the BSCF lattice leaving a concentration gradient BSCF-D shell outside the BSCF. Two points ensure no impurities form at the cathode|SDC interface. Firstly, microwave plasma can heat the surface of BSCF backbone to ~1800°C in a few second, so total heating time can be less than 1 h. Secondly, only BSCF can be heated under given power (300W) due to the selective heating characteristic of microwave plasma.

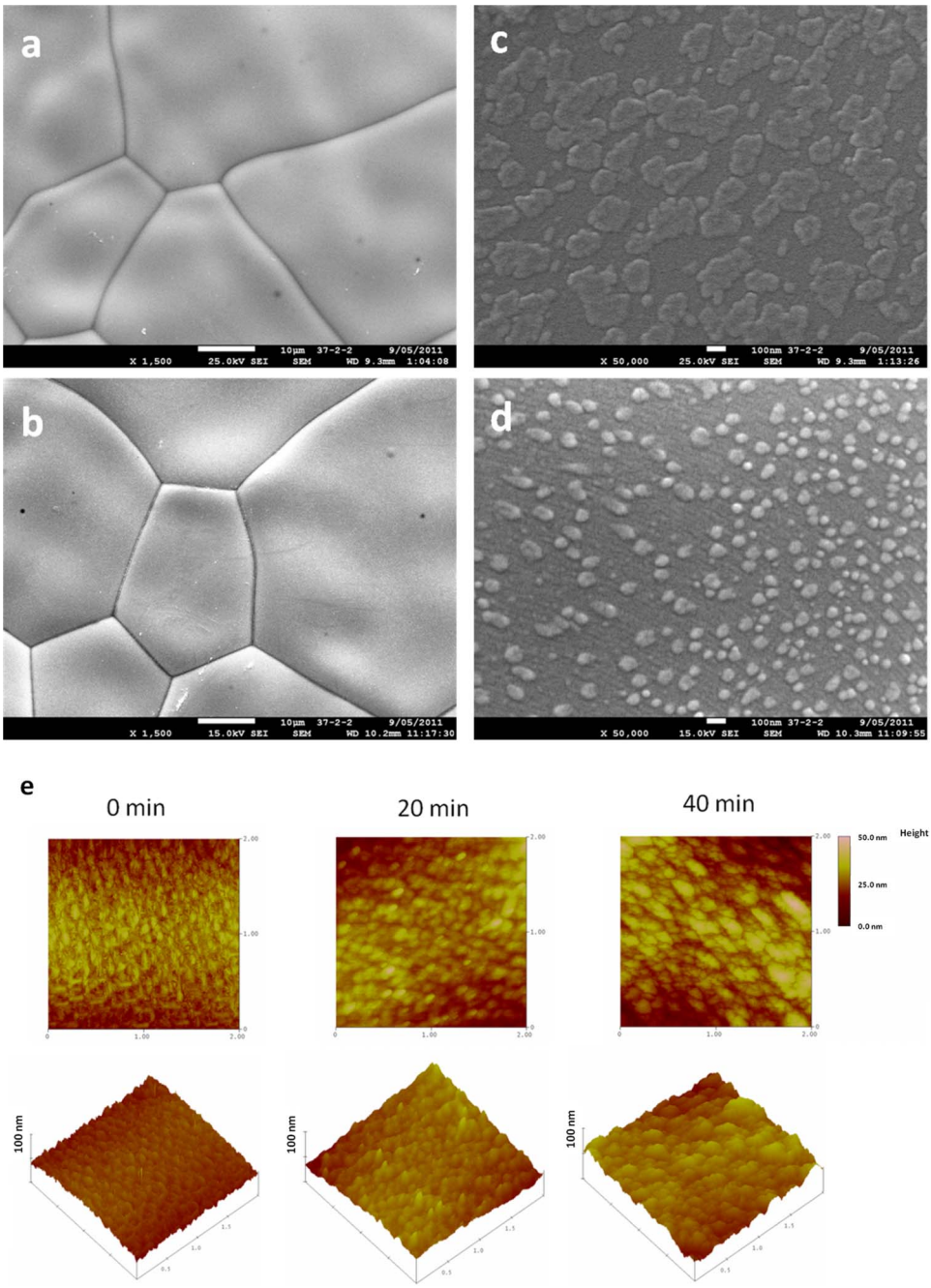

Figure 2 | Morphologies of surface of the fresh BSCF and treated BSCF. (a, c) FESEM images of the fresh BSCF, and (b, d) the BSCF treated under microwave plasma for 40 min. (e) AFM images of the surface of the fresh BSCF (0 min) and the BSCF treated under microwave plasma for 20 and 40 min. The scan area is 2.0×2.0 μm.

surface are shown in **Figure 2e**. It is clearly seen that the surface of fresh BSCF is flatter than the treated ones. The root-mean-square (rms) roughness of the fresh BSCF surface is 4.8 nm. The roughness increases to 5.3 and 7.1 nm after treatment for 20 and 40 min, respectively. Small grains are also observed by AFM after the treatment. The grain heights are 13.0 and 15.2 nm for the samples treated for 20 and 40 min.

The composition change of the materials from outer surface to a depth of ~130 nm was investigated by XPS using Ar^+ etching technique with an etching speed of ~1 nm min^{-1}. The etching experiment was firstly carried out on BSCF sample to identify whether the Ar^+ etching process induces the structure change of the BSCF. The intensity of the peaks for Ba*4d*, Sr*3d* and Co*3p* is unchanged with increasing etching depth (**Figures 3a and b**), indicating no structure change induced by Ar^+ etching. For the microwave plasma treated BSCF, the intensity of Co*3p* peak remainss unchanged, while the intensity of Ba*4d* and Sr*3d* increases with increasing etching depth (**Figure 3c**). This suggests only Ba and Sr elements evaporate from BSCF lattice under microwave plasma treatment. The concentration change of Ba, Sr and Co element (**Figure 3d**) reveals the formation of concentration gradient BSCF-D shell (~25 nm) on the BSCF core after 40-min treatment. The bulk compositions determined by XPS for both fresh and treated BSCF samples are very similar to each other, indicating the treatment has no influence on the bulk of the material.

Electrochemical properties. Electrocatalytic activity of the heterostructured cathode was tested by electrochemical impedance

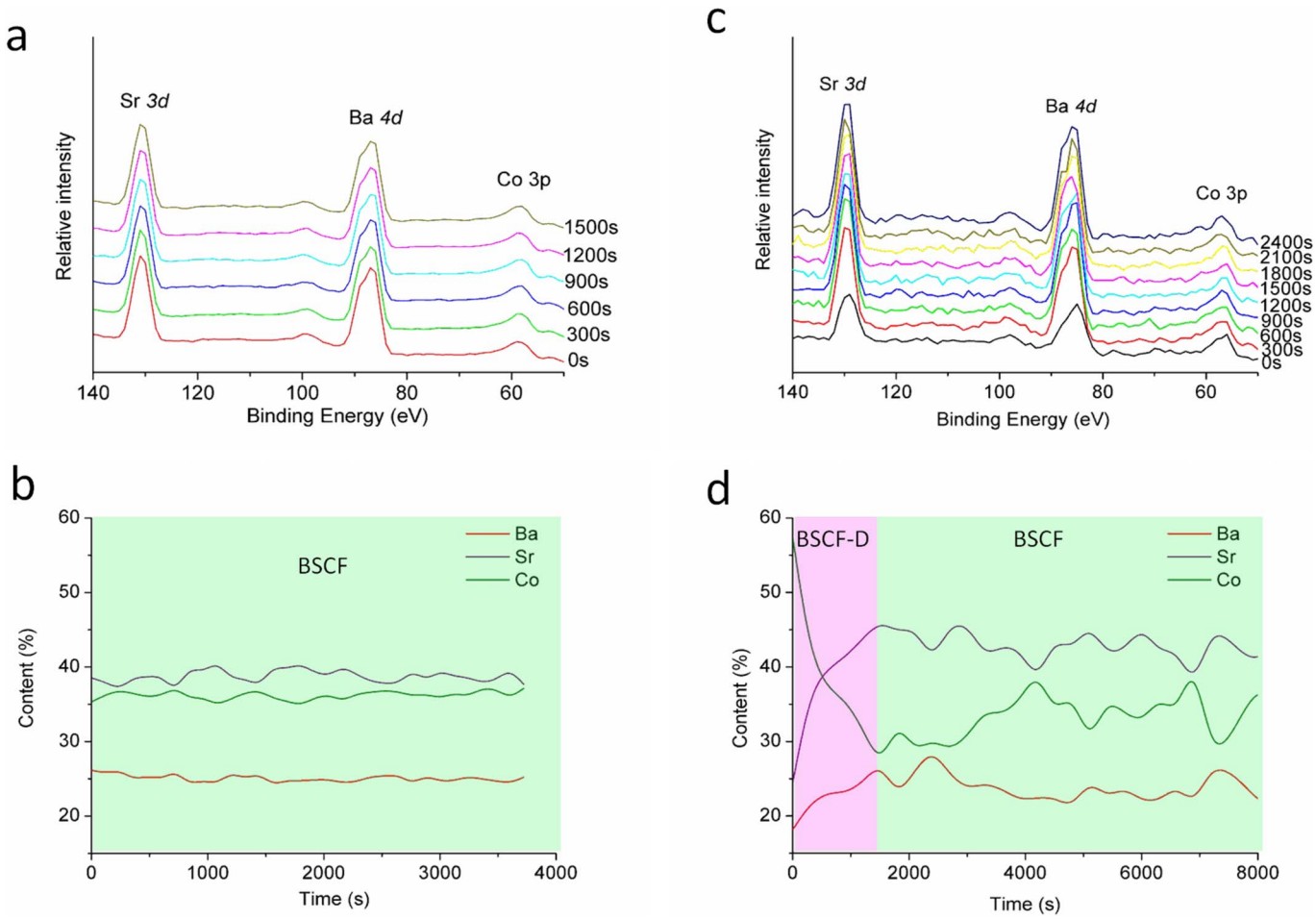

Figure 3 | Composition analysis of the fresh BSCF and treated BSCF. XPS profiles of (a) the pristine BSCF and (c) the BSCF treated for 40 min under microwave plasma as a function of etching time. Depth plots of elemental composition for (b) the pristine BSCF and (d) the treated BSCF after Ar^+ etching at a rate of ~1 nm min^{-1}. Because all the characteristic peaks of Fe are overlapped with other elements, we did not analyse the content of Fe here.

spectroscopy (EIS) on a symmetric cell with configuration of electrode|SDC|electrode. The typical Nyquist impedance curves for the pristine BSCF and core-shell structured cathodes tested at 600°C are shown in **Figure 4a**. The difference between real axes intercepts of the impedance plot is the electrode polarization resistance (R_p). The R_p of the pristine BSCF cathode is 0.162 **Ω** cm^2 at 600°C. After microwave plasma treatment, the R_ps are reduced to 0.061–0.079 **Ω** cm^2 depending on the treating time, which means more than ~100% enhancement of electrochemical performance is achieved on the heterostructured cathode. Such enhancement can further increase to ~220% and ~330% at 550 and 500°C on the heterostructured cathode treated under microwave plasma for 40 min operating (**Figure 4b**). An ASR of 0.143 **Ω** cm^2 is achieved at 550°C, which is lower than the target value of 0.15 **Ω** cm^2 proposed by Steele for SOFCs operating at reduced temperature[24]. The R_p of the heterostructured cathode is unchanged after heating it at 550°C for 200 h (**Figure S4, supporting information**). The decrease of activity of the cathode treated for 80 min is likely due to the formation of impurity substances caused by the deep decomposition of BSCF.

Further analysis is performed on the EIS curves to understand the role of concentration gradient BSCF-D shell in performance enhancement. There are at least two independent steps involved in the ORR on the BSCF cathode, reflected by two depressed arcs in impedance curves as shown in **Figure 4a**. The arc at high frequency is related to the charge-transfer process (R_{E1}), while the one at low frequency is related to oxygen surface process (R_{E2}) including oxygen adsorption-desorption of oxygen, oxygen diffusion at the gas-cathode interface and surface diffusion of intermediate oxygen species[19]. The deconvolution results for R_{E1} and R_{E2} at 600°C are listed in **Table S1**. The R_{E1} almost keeps at a constant value for all the samples, but the R_{E2} decreases to ~0.039 **Ω** cm^2 from ~0.138 **Ω** cm^2 (Enhancement is about ~250%) after microwave plasma treatment for 40 min. This suggests that the formed concentration gradient shell can decrease the resistance of oxygen surface process.

Discussion

The oxygen surface exchange process is the rate-determining step (RDS) of ORR for the pristine BSCF[19]. Introduction of A-site cations deficiency into BSCF was proved to accelerate its oxygen surface process[17,18], but formation of impurities at the cathode|electrolyte interface was also observed to be detrimental to the charge-transfer process. In the present study, a nano-sized BSCF-D functional shell can be simply obtained by microwave plasma. Application of such a shell outside the BSCF successfully circumvents the problem caused by the serious phase reaction between this material and SDC electrolyte, leading to the improved oxygen surface process without impact on the charge-transfer process.

Another merit of microwave plasma treatment is that the shell is concentration gradient. It was reported that the structural mismatch between the core and the shell may lead to the formation of voids between the core and the shell, because the different degrees of shrinkage may lead to gradual separation of the core and shell[22]. This problem can be solved by employing concentration gradient shell outside the core[25]. In our previous study, very different thermal

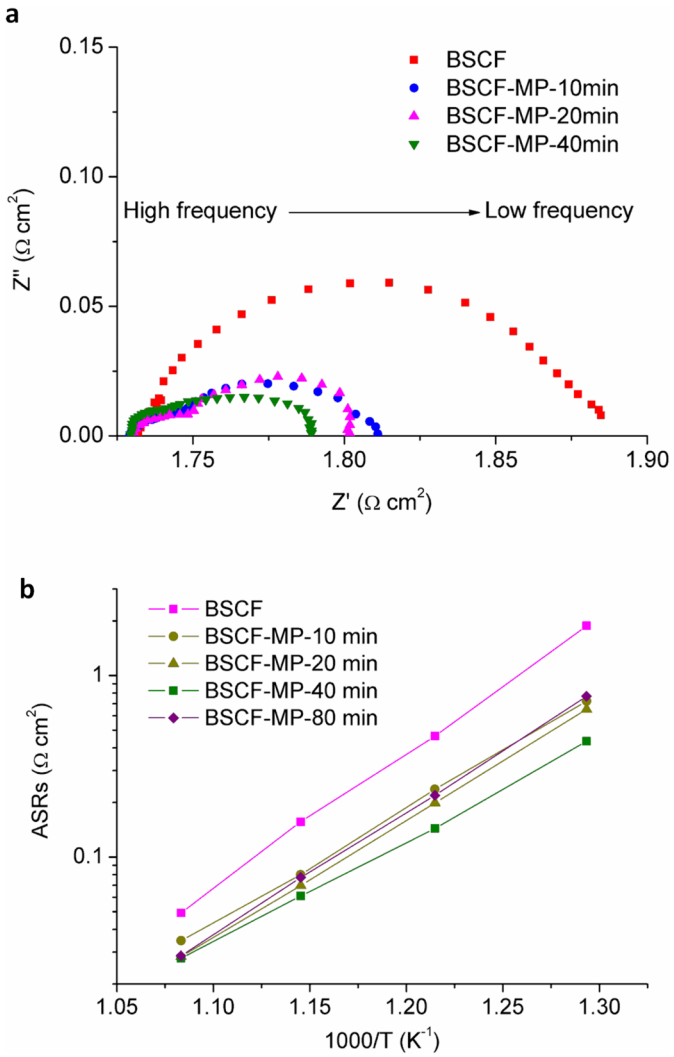

Figure 4 | Electrochemical performance of the heterostructured cathode. (a) Typical impedance spectra tested at 600°C for the fresh BSCF and the BSCF cathodes treated under microwave plasma (MP) for 10, 20 and 40 min. (b) Arrhenius plots of ASRs for the fresh BSCF and the BSCF cathodes treated for 10, 20, 40 and 80 min.

expansion coefficients (TEC) were observed on between BSCF-D and BSCF. If the concentration of Ba and Sr elements changes abruptly, the mismatch between BSCF-D shell and BSCF core is likely to occur[18].

It has been reported that A-site deficient perovskite oxides may show enhanced electrochemical performance, oxygen permeability, magnetic property, dielectric constant or sintering behaviour compared to the stoichiometric ones, such as $(La_{0.6}Sr_{0.4})_{1-x}Co_{0.2}Fe_{0.8}O_{3-\delta}$ (ref. 27), $Ba_{1-x}Co_{0.7}Fe_{0.2}Nb_{0.1}O_{3-\delta}$ (ref. 28), $Sr_{0.8}Ce_{0.1}Fe_{0.7}Co_{0.3}O_{3-\delta}$ (ref. 29), $Ba_{1-y}Ln_{2y/3}$ $Zr_{0.09}Ti_{0.91}O_3$ (Ln = La, Pr, Nd) (ref. 30), and $Ba_{1-x}Ce_{0.4}Zr_{0.4}Y_{0.2}O_{3-\delta}$ (ref. 31). It is noteworthy that here we only express an example of enhancement of the oxygen reduction activity on a cathode material. It is also possible to use the microwave plasma treatment to prepare heterostuctures on other perovskite oxides for various applications. The A-site cations of perovskite are rare-earth and/or alkaline-earth elements, while B-site cations are transition metals. Enthalpy of vaporization (H_v) of an alkaline-earth or rare-earth element (e.g. the H_v of Ba, Sr, Ca and Sm is 140.3, 136.9, 154.7 and 165 kJ mol^{-1} respectively) is usually much lower than that of a transition metal (e.g. the H_v of Co, Fe, Cu, Ce and Ni is 377, 340, 300.4, 398 and 377.5 kJ mol^{-1} respectively) (ref. 26). This means that A-site cations are easily evaporated from perovskite lattice to form A-site deficient perovskite oxide. It is expected that the enhanced performance can be realized by using microwave plasma treatment in the abovementioned applications.

In summary, we have developed a 3D heterostructured cathode by treating BSCF cathode under microwave plasma. The concentration gradient BSCF-D shell can be obtained on the BSCF core without formation of impurities at the cathode|electrolyte interface. The activity of the cathode is enhanced by over 200% at low temperature due to the significantly improved oxygen surface process. This method can be widely used in various applications that use ceramic materials as the components.

Experimental section. BSCF powder was synthesized by combined EDTA-citrate complexing process as described in ref. 18. BSCF porous layer was prepared by wet powder spraying method. BSCF slurry for spray deposition was prepared by dispersing BSCF powder with a premixed solution of glycerol, and isopropyl alcohol followed by rapid mixing and milling in an agate mortar for 0.5 hours by hand. The symmetrical cell with the configuration of BSCF|SDC|BSCF was fabricated by spraying BSCF slurry onto both surfaces of SDC disk and calcining the sprayed cells in air at 1000°C for 2 hours.

The plasma treatment of BSCF|SDC|BSCF cells was carried out in a vertical quartz tube located inside the microwave waveguide cavity. The microwave magnetron provides 300 W of power at a fixed frequency 2.45 GHz. The temperature of the sample was monitored by an infrared radiation thermometer.

Phase structural analysis of the samples was carried out using XRD (Bruker D8 Advance). The surface morphology of the BSCF was studied on BSCF pellets (sintered at 1000°C for 2 h) before and after microwave plasma treatment by FESEM (JEOL 7001) with an embedded EDX system and AFM (SPI 3800 SII Nano Technology Inc.). The composition change with the depth was analyzed by XPS (Kratos Axis ULTRA) using Ar^+ etching technique. The etching rate was estimated at ~1 nm min^{-1}.

The EIS of the symmetric cells were obtained using an Autolab (PGSTAT30 electrochemical workstation). The frequency range was 0.1 Hz to 100 kHz and the signal amplitude was 10 mV under open cell voltage conditions.

1. Steel, B. C. H. & Heinzel, A. Materials for fuel-cell technologies. *Nature* **414**, 345–352 (2001).
2. Minh, N. Q. Ceramic fuel cells. *J. Am. Ceram. Soc.* **76**, 563–588 (1993).
3. Singhal, S. C. Advances in solid oxide fuel cell technology. *Solid State Ionics* **135**, 305–313 (2000).
4. Brett, D. J. L., Atkinson, A., Brandon, N. P. & Skinner, S. J. Intermediate temperature solid oxide fuel cells. *Chem. Soc. Rev.* **37**, 1568–1578 (2008).
5. Hibino, T. *et al.* A low-operating-temperature solid oxide fuel cell in hydrocarbon-air mixtures. *Science* **288**, 2031–2033 (2000).
6. Yang, L. *et al.* Enhanced sulfur and coking tolerance of a mixed ion conductor for SOFCs: $BaZr_{0.1}Ce_{0.7}Y_{0.2-x}Yb_xO_{3-\delta}$. *Science* **326**, 126–129 (2009).
7. Zhou, W. & Zhu, Z. H. The instability of solid oxide fuel cells in an intermediate temperature region. *Asia-Pac. J. Chem. Eng.* **6**, 199–203 (2011).
8. Anderson, H. U. Review of p-type doped perovskite materials for SOFC and other applications. *Solid State Ionics* **52**, 33–41 (1992).
9. Peña, M. A. & Fierro, J. L. G. Chemical structures and performance of perovskite oxides. *Chem. Rev.* **101**, 1981–2018 (2001).
10. Jacobson, A. J. Materials for solid oxide fuel cells. *Chem. Mater.* **22**, 660–674 (2010).
11. Orera, A. & Slater, P. R. New chemical systems for solid oxide fuel cells. *Chem. Mater.* **22**, 675–690 (2010).
12. Tarancón, A., Burriel, M., Santiso, J., Skinner, S. J. & Kilner, J. A. Advances in layered oxide cathodes for intermediate temperature solid oxide fuel cells. *J. Mater. Chem.* **20**, 3799–3813 (2010).
13. Fleig, J. On the width of the electrochemically active region in mixed conducting solid oxide fuel cell cathodes. *J. Power Sources* **105**, 228–238 (2002).
14. Adler, S. B. Factors governing oxygen reduction in solid oxide fuel cell cathodes. *Chem. Rev.* **104**, 4791–4844 (2004).
15. Shao, Z. P. & Haile, S. M. A high-performance cathode for the next generation of solid-oxide fuel cells. *Nature* **431**, 170–173 (2004).
16. Baumann, F. S., Fleig, J., Habermeier, H. U. & Maier, J. $Ba_{0.5}Sr_{0.5}Co_{0.8}Fe_{0.2}$ $O_{3-\delta}$ thin film microelectrodes investigated by impedance spectroscopy. *Solid State Ionics* **177**, 3187–3191 (2006).

17. Ge, L. *et al.* Properties and performance of A-site deficient $(Ba_{0.5}Sr_{0.5})_{1-x}Co_{0.8}Fe_{0.2}O_{3-\delta}$ for oxygen permeating membrane. *J. Membr. Sci.* **306**, 318–328 (2007).
18. Zhou, W., Ran, R.an, Shao, Z. P., Jin, W. Q. & Xu, N. P. Evaluation of A-site cation-deficient $(Ba_{0.5}Sr_{0.5})_{1-x}Co_{0.8}Fe_{0.2}O_{3-\delta}$ (x>0) perovskite as a solid-oxide fuel cell cathode. *J. Power Sources* **182**, 24–31 (2008).
19. Zhou, W. *et al.* Barium- and strontium-enriched $(Ba_{0.5}Sr_{0.5})_{1+x}Co_{0.8}Fe_{0.2}O_{3-\delta}$ oxides as high-performance cathodes for intermediate-temperature solid-oxide fuel cells. *Acta Mater.* **56**, 2687–2698 (2008).
20. Zhou, W. *et al.* Effect of a reducing agent for silver on the electrochemical activity of an $Ag/Ba_{0.5}Sr_{0.5}Co_{0.8}Fe_{0.2}O_{3-\delta}$ electrode prepared by electroless deposition technique. *J. Power Sources* **186**, 244–251 (2009).
21. Zhou, W. *et al.* Electrochemical performance of silver-modified $Ba_{0.5}Sr_{0.5}Co_{0.8}Fe_{0.2}O_{3-\delta}$ cathodes prepared via electroless deposition. *Electrochim. Acta* **53**, 4370–4380 (2008).
22. Sun, Y.-K. *et al.* Synthesis and characterization of $Li[(Ni_{0.8}Co_{0.1}Mn_{0.1})_{0.8}-(Ni_{0.5}Mn_{0.5})_{0.2}]O_2$ with the microscale core–shell structure as the positive electrode material for lithium batteries. *J. Am. Chem. Soc.* **127**, 13411–13418 (2005).
23. Guo, X. X. & Maier, J. Ionically conducting two-dimensional heterostructures, *Adv. Mater.* **21**, 2619–2631 (2009).
24. Steele, B. C. H. Survey of materials selection for ceramic fuel cells II. Cathodes and anodes. *Solid State Ionics* **86–88**, 1223–1234 (1996).
25. Sun, Y.-K. *et al.* High-energy cathode material for long-life and safe lithium batteries. *Nat. Mater.* **8**, 320–324 (2009).
26. Dean, J. A. Lange's Handbook of Chemistry 15th Edition, McGraw-Hill, Inc, New York, (1999).
27. Hansen, K. K. & Vels Hansen, K. A-site deficient $(La_{0.6}Sr_{0.4})_{1-s}Fe_{0.8}Co_{0.2}O_{3-\delta}$ perovskites as SOFC cathodes . *Solid State Ionics* **178**, 1379–1384 (2007).
28. Zhao, H. L. *et al.* Oxygen permeability of A-site nonstoichiometric $Ba_xCo_{0.7}Fe_{0.2}Nb_{0.1}O_{3-\delta}$ perovskite oxides. *Solid State Ionics* **181**, 354–358 (2010).
29. Carvalho, M. D. *et al.* Magnetic studies on $Sr_{0.8}Ce_{0.1}Fe_{0.7}Co_{0.3}O_{3-\delta}$ perovskite. *Solid State Sci.* **8**, 444–449 (2006).
30. Ostos, C. *et al.* Synthesis and characterization of A-site deficient rare-earth doped $BaZr_xTi_{1-x}O_3$ perovskite-type compounds. *Solid State Sci.* **11**, 1016–1022 (2009).
31. Guo, Y. M., Ran, R., Shao, Z. P. & Liu, S. M. Effect of Ba nonstoichiometry on the phase structure, sintering, electrical conductivity and phase stability of $Ba_{1\pm x}Ce_{0.4}Zr_{0.4}Y_{0.2}O_{3-\delta}$ ($0\leq x\leq 0.20$) proton conductors. *Int. J. Hydrogen Energy* **36**, 8450–8460 (2011).

Acknowledgements

Prof Zongping Shao acknowledges the support of "China National Funds to Distinguished Young Scientists"under contract No. 51025209.

Author contributions

W.Z. Z.P.S. and Z.H.Z. drafted and revised the manuscript, conceptualized the study. F.L.L. performed synthesis, characterizations and analyses. J.L.C. performed microwave plasma treatment of the samples.

Additional information

Supplementary information accompanies this paper at http://www.nature.com/scientificreports

Competing financial interests: The authors declare no competing financial interests.

How to cite this article: Zhou, W., Liang, F., Shao, Z., Chen, J. & Zhu, Z. Heterostructured electrode with concentration gradient shell for highly efficient oxygen reduction at low temperature. *Sci. Rep.* **1**, 155; DOI:10.1038/srep00155 (2011).